Biomaterials 61 (2015) 290–298

Contents lists available at ScienceDirect

Biomaterials

journal homepage: www.elsevier.com/locate/biomaterials

Impairing the radioresistance of cancer cells by hydrogenated nanodiamonds

Romain Grall [a], Hugues Girard [b], Lina Saad [a], Tristan Petit [b], Céline Gesset [b], Mathilde Combis-Schlumberger [b], Vincent Paget [a], Jozo Delic [a], Jean-Charles Arnault [b], Sylvie Chevillard [a, *]

[a] Commissariat à l'Energie Atomique et aux Energies Alternatives (CEA), IRCM, Laboratory of Experimental Cancerology (LCE), Fontenay aux Roses, France
[b] Commissariat à l'Energie Atomique et aux Energies Alternatives (CEA), LIST, Diamond Sensors Laboratory, Gif-sur-Yvette, France

ARTICLE INFO

Article history:
Received 9 February 2015
Received in revised form
13 May 2015
Accepted 18 May 2015
Available online 20 May 2015

Keywords:
Hydrogenated nanodiamonds (H-NDs)
Radiation sensitization
Oxidative stress
γ-H2AX
Senescence

ABSTRACT

Hydrogenated nanodiamonds (H-NDs) exhibit a negative electron affinity that confers a high reactivity with oxygen species and a positive charge in aqueous solutions. It allows electron emission from H-NDs following irradiation by photons and in consequence may enhance the effects of radiation on cancer cells.

By using three human radioresistant cancer cell lines, we showed a potentialization of cytotoxicity after a co-exposure to H-NDs and irradiation; an event occurring through the induction of DNA damage and reactive oxygen species. This occurred together with a decrease in cell impedance, the activation of G_1/S, an unlocking of G_2 cell cycle check-points and early low cell death rate. At later stage of exposure, persistent increases in heterochromatinization, large γ-H2AX foci and β-galactosidase activity were detected providing evidence of cells' entrance into senescence. Similar potentialization was observed with neocarzinostatin (NCS), a radiomimetic drug.

This original finding underlines a wide clinical potential of H-NDs to intensify radiation effects on radio-resistant cancer cells.

© 2015 The Authors. Published by Elsevier Ltd. This is an open access article under the CC BY license (http://creativecommons.org/licenses/by/4.0/).

1. Introduction

Nanodiamonds (NDs) have gained increasing attention as an efficient drug delivery nanoplatform, for both diagnostic and therapeutic purposes [1–3]. Several *in vitro* [4–6] and *in vivo* [7–9] studies have shown that NDs are non-cytotoxic with an enhanced cell tolerance compared to other carbon nanoparticles. Depending on their production method, NDs are scalable with sizes ranging from 100 nm down to 5 nm. Moreover, luminescent nitrogen-vacancy (N–V) color photostable centers can be generated in the diamond lattice of NDs [4,10] and such fluorescent NDs can act as diagnostic biomarkers when functionalized with specific probes.

Because of these combined properties, NDs have attracted growing interest as nano-vectors. The carbon-related surface chemistry of these particles provides an efficient and versatile platform for bio-conjugation that can be used in therapeutic applications [11–15]. For instance, carboxylated nanodiamonds exhibit a strong negative zeta potential when dispersed in water at a pH > 5 [16,17]. On the other hand, surface treatments such as plasma hydrogenation [18,19] or surface graphitization lead to positive zeta potential in aqueous suspension [16,20]. In both cases, the diameter of the particle is not affected. As a consequence, the tuning of the ND surface charge allowed the electrostatic loading of biomolecules such as siRNAs [11,21,22] or drugs including plant bioactive metabolites [23]. Another characteristic of NDs provided by their surface chemistry concerns their electronic properties. Indeed, hydrogenated detonation NDs have a negative electron affinity (NEA) that is similar to hydrogenated diamond films [24]. This property induces a strong interaction with water molecules leading to transfer doping [20]. This p-type conductivity of H-NDs was recently measured [25].

Our present study findings demonstrate that hydrogenated nanodiamonds (H-NDs) can act as active nanoparticles. Bearing an NEA that enables the emission of electrons, and when surrounded

* Corresponding author.
E-mail addresses: romain.grall@cea.fr (R. Grall), hugues.girard@cea.fr (H. Girard), lina2321986@hotmail.com (L. Saad), tristan.petit@helmholtz-berlin.de (T. Petit), celine.gesset@cea.fr (C. Gesset), mathilde.combis-schlumberger@centraliens.net (M. Combis-Schlumberger), vincent.paget@cea.fr (V. Paget), jozo.delic@cea.fr (J. Delic), jean-charles.arnault@cea.fr (J.-C. Arnault), sylvie.chevillard@cea.fr (S. Chevillard).

http://dx.doi.org/10.1016/j.biomaterials.2015.05.034
0142-9612/© 2015 The Authors. Published by Elsevier Ltd. This is an open access article under the CC BY license (http://creativecommons.org/licenses/by/4.0/).

with oxygen-related adsorbents, H-NDs may act as an efficient source of reactive oxygen species (ROS) when excited with sub-bandgap energies, from UV to X-rays. Indeed, our experiments revealed that H-NDs can have a radiosensitizing effect on cancer cells by generating ROS in addition to those generated by ionizing irradiation. By testing radiation resistant human cancer cell lines, we established a higher generation of ROS leading to a greater cytotoxicity and genotoxicity when intracellular H-NDs were exposed to γ-rays as compared to radiation or H-NDs alone. This radiation sensitizing effect of H-NDs results in sustained DNA double strand breaks (DSBs), a cell cycle check-point switch from G_2/M to a G_1/S arrest, and finally in cell senescence. Of note, among the cancer cell lines we tested, those derived from a breast cancer were found to express a deregulated Ku70 gene involved in DSB DNA repair through non-homologous end-joining (NHEJ), which is normally active throughout all phases of cell cycle. In contrast, the renal cancer cell line is wild type for this gene. Hence, considering that single strand breaks (SSB) result in DSBs if not repaired, or if misrepaired, and that senescence was triggered in all cell lines tested, our data strongly suggest that ROS-induced G_1/S arrest is the specific event leading to senescence induction. Taken together, our data emphasize the wide potential of H-NDs in the development of new therapeutic strategies combining these nanoparticles with radiotherapy.

2. Results

2.1. Physical and chemical characteristics of H-NDs

Electron emission properties are conferred on NDs by the presence of hydrogenated terminations on their surface [20]. Such terminations can be efficiently created by plasma hydrogenation as described elsewhere [19]. Size and Zeta potential of H-NDs have been characterized after being dispersed in aqueous suspension by sonication (Table 1). For this purpose, a suspension of H-NDs at 1 mg/mL was used. As reported in our previous study [20], hydrogenated NDs dispersed in an aqueous solution are highly reactive toward oxygenated species, which leads to a conductive surface layer. A positive Zeta potential was measured in our current study (44 mV at pH = 7) consistent with our previous report [20].

The H-NDs were then dispersed in DMEM cell culture medium. The corresponding suspension exhibited an increase of the hydrodynamic radius whilst the Zeta potential dropped to −7 mV. These latter effects are likely related to adsorption of a corona of proteins on the H-NDs surface that might be at the origin of the slight aggregation [26,27].

2.2. Real-time cellular index (impedance)

We screened the cytotoxicity of H-NDs, combined or not with radiation exposure, by monitoring cell impedance (RTCA xCELLigence®) [28,29]. The cellular index as a function of time reflects a real-time integrative measure of the morphology, proliferation, growth and membrane potential of cells. Importantly, impedance cell dedicated culture plates are compatible with γ-irradiation exposure and H-NDs alone do not interfere with this measurement [30,31]. Thus, the impedance value reflecting global cell "health" under standard *in vitro* cell culture conditions, was measured simultaneously for untreated (controls), irradiated, and H-ND-treated cells, and also for cells treated with both H-NDs and irradiation. We selected three cell lines: two breast cancer derived cell lines created in our laboratory harboring the conditional expression of Ku70, an essential protein in the classical NHEJ DNA repair pathway ($ZR75.1_{Ku70wt}$ and $ZR75.1_{Ku70mut}$; Bouley et al., submitted) and a kidney cancer cell line (Caki-1).

In agreement with the previously established radioresistance of these cell lines by other approaches, they could also be considered resistant to 4 Gy irradiation using the xCELLigence® assay (Fig. 1). The evolution of the cellular index of the three untreated cell lines throughout 180 h was quite similar, indicating their close doubling times (Fig. 1). Cells were exposed to three different concentrations of H-NDs: 10 μg/mL, 50 μg/mL and 100 μg/mL corresponding to 6 μg/cm^2 32 μg/cm^2 and 64 μg/cm^2, respectively. However, following single cell treatments, this method appeared less robust and divergent results were obtained between the tested cell lines since the cell indexes unexpectedly but significantly increased. The Caki-1 cells treated only by irradiation exhibited a higher (2-fold, see Table 2) cell index similar to the breast cancer derived cell lines treated by H-NDs alone (Fig. 1). This of course could not account for real cell behavior improved by these treatments but rather indicated a morphological change (i.e. cell shrinkage, not shown), and thus reflected global changes in the extracellular matrix (cell adhesion) without affecting long term cell proliferation or growth (as further validated by specific experimental approaches described below).

Overall, this new methodology showed some limitations in assessing multiparametric cellular toxicity (i.e. cell treatment affecting cell morphology and adhesion in addition to membrane potential, cell mass and proliferation for which it was initially dedicated). Nevertheless, the xCELLigence® approach allowed us to conclude that the potentially effective dose of H-NDs combined with irradiation or with the radio-mimetic drug neocarzinostatin could be as low as 6 μg/cm^2. Thus, this dose was chosen to further characterize the biological effects of H-NDs through conventional and validated methods. Using irradiated cells as the controls (rather than untreated cells), co-exposure of cells to the same concentrations of H-NDs and to 4 Gy irradiation led to a decreased cellular index for the two more radio-resistant cells (Caki-1 and $ZR75.1_{Ku70mut}$). This observation was relevant to the level of induced cellular toxicity. Indeed, an identical increased effect was evidenced when the cells were simultaneously treated by H-NDs and the neocarzinostatin radiomimetic at 3.3 nM, a dose chosen as the equivalent to irradiation at 4 Gy (see Supplementary Data 1). This last observation is in agreement with the observed morphological alterations induced by irradiation that contributed to increased cell impedance since neocarzinostatin induces oxidative stress like irradiation (see below).

Thus, to further explore the biological effects of H-NDs, we next evaluated cell death, cell cycle control, the induction of ROS and DNA damage by applying this dose of H-NDs. We also assessed

Table 1
Polydispersity Indexes after sonication, Dynamic Light Scattering, and Zeta Potential of 1 mg/mL H-NDs suspended in water and complete media.

Suspension medium		Polydispersity index (PDI)	Dynamic light scattering (DLS)			Zeta potential	
			Hydrodynamic radius (nm)	%Number	SD	Value	SD
Water	Peak 1	0.311	16	100	±5.5	44	±4.92
Complete DMEM[a]	Peak 1	0.590	20	89.4	±3.3	−7	±0
	Peak 2		53	10.6	±35.14		

[a] DMEM medium with 10% vol/vol FBS (pH = 7).

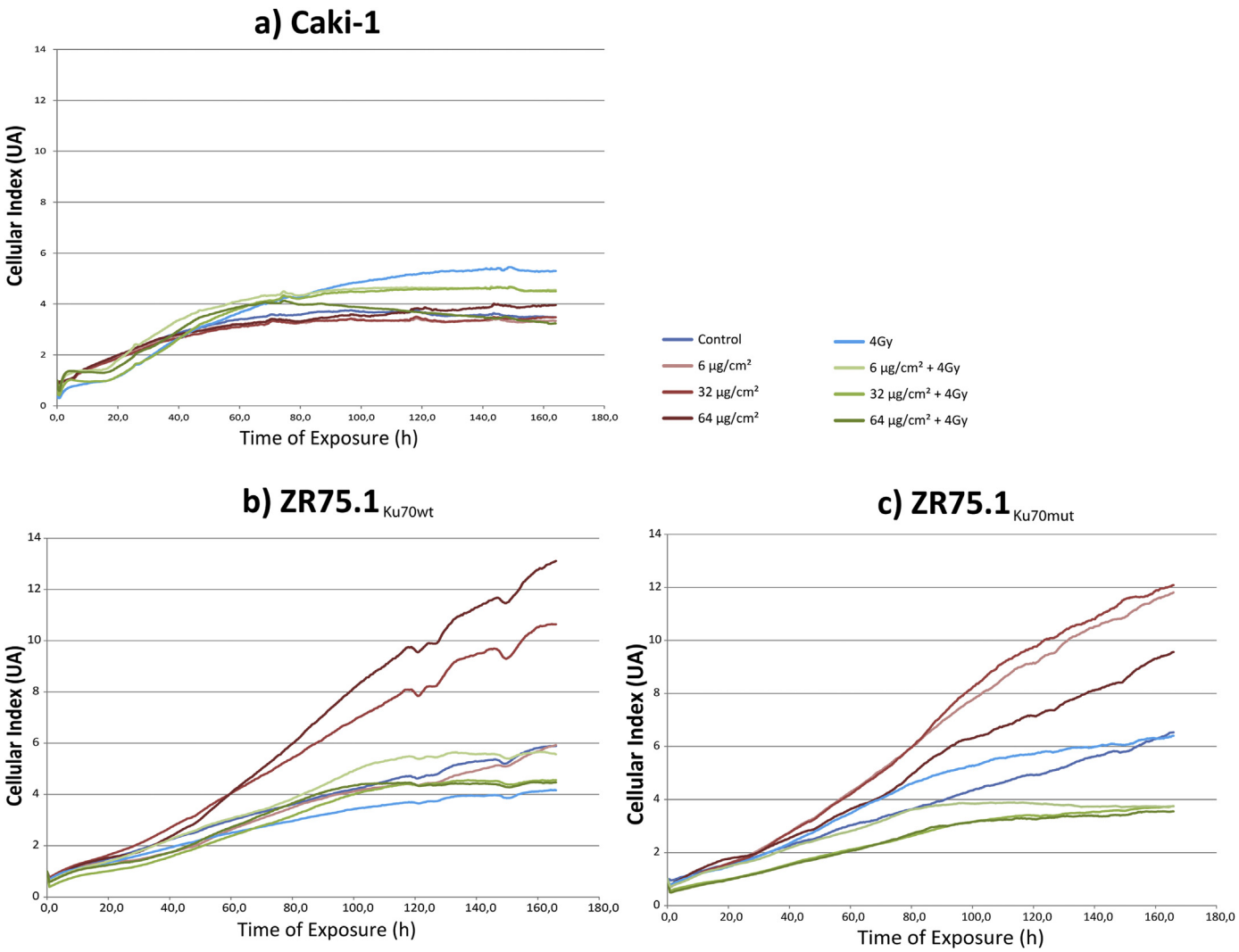

Fig. 1. Real-time monitoring of cells exposed to H-NDs and/or irradiation to measure the cell index. Real-time monitoring of the cell index in a) Caki-1, b) ZR75.1$_{Ku70wt}$, and c) ZR75.1$_{Ku70mut}$ cells exposed to three dose levels of H-NDs with or without irradiation (4 Gy). Impedance measurements (one representative experiment among three independent experiments is shown) were carried out for 170 h and the cell index values were normalized at time 0 to avoid inter-well variability prior to the addition of nanoparticles. "Control" and "4 Gy" cells were not exposed to H-NDs.

whether cell growth arrest was due to entry into irreversible senescence.

2.3. Cell death assessment

The cytotoxicity of H-NDs alone or in combination with ionizing irradiation was analyzed by measuring trypan blue exclusion which indicates cell viability (Fig. 2). As expected, since we specifically tested a radiation resistant cell line, ionizing irradiation exposure at a 4 Gy dose did not significantly affect cell viability up to 72 h post-treatment. H-NDs alone induced only a 20% rate of cell death in the breast cancer lines and did not affect Caki-1 cell viability at all. However, a combined exposure of H-NDs (6 µg/cm^2) and irradiation (4 Gy), significantly increased the rate of cell death in all three cell lines as compared to each single exposure (irradiation or H-NDs alone) with a stronger effect being observed for Caki-1 and ZR75.1$_{Ku70mut}$ cells (Fig. 2).

2.4. Cell cycle check-point activation (flow cytometry)

Considering that ionizing irradiation activates cell cycle checkpoints [32,33], we addressed whether a co-exposure to H-NDs and irradiation would activate specific cell cycle checkpoints. Indeed, upon exposure to radiation alone, an accumulation of cells in G_2/M phase was observed for all three cell lines at 24 h after exposure. This was expected since these three cell lines express all *TP53* wild type. The intensity of the G_2 blockage depended on the radiation sensitivity of each cell line. Being the most resistant line, Caki-1 cells displayed a higher proportion of G_2/M arrested cells followed by ZR75.1$_{Ku70mut}$ and ZR75.1$_{Ku70wt}$ (Fig. 3). It should be noted that Caki-1 cells exhibited an additional blockage in G_1 phase. Interestingly, while exposure to H-NDs alone did not modify the cell cycle distribution of the three treated cell lines, the co-exposure to H-NDs and irradiation induced a partial lifting of G_2/M arrest leading to a higher proportion of cells with a G_1/S blockage, as compared to irradiation alone.

2.5. Early intracellular ROS levels

This prompted us to analyze the intracellular ROS level in Caki-1 cells which were selected for having a higher level of radiation resistance than the other two cell lines analyzed. As shown in

Table 2
Compilation of final cell event ratios. The ratios between the sample and control values were calculated for each experimental condition. The time points at the maximal observed effects were chosen. Irradiation (IR, 4Gy) only compares results between irradiation and control. IR + H-NDs (hydrogenated nanodiamonds) compares results between double cell treatment and IR only. NI, Non Irradiated.

xCELLigence	*Caki-1*	Time 160 h	**NI**				**IR**	**IR + H-NDs**		
			6 μg/cm^2	64 μg/cm^2	96 μg/cm^2		0	6 μg/cm^2	64 μg/cm^2	96 μg/cm^2
			0.95	0.87	0.83		1.39	0.86	0.85	0.62
	ZR75.1$_{Ku70wt}$	Time 160 h	**NI**				**IR**	**IR + H-NDs**		
			6 μg/cm^2	64 μg/cm^2	96 μg/cm^2		0	6 μg/cm^2	64 μg/cm^2	96 μg/cm^2
			1.52	1.83	1.62		0.71	1.24	1.04	1.03
	ZR75.1$_{Ku70mut}$	Time 160 h	**NI**				**IR**	**IR + H-NDs**		
			6 μg/cm^2	64 μg/cm^2	96 μg/cm^2		0	6 μg/cm^2	64 μg/cm^2	96 μg/cm^2
			1.02	1.23	0.89		0.46	0.79	0.77	0.75
Cell Cycle	*Caki-1*	Time 24 h	**H-NDs**			**IR**			**IR + H-NDs**	
			G1	S	G2	G1	S	G2	G1	S	G2
			1.00	0.88	1.01	0.68	0.22	2.23	0.73	0.71	1.78
	ZR75.1$_{Ku70wt}$	Time 12 h	**H-NDs**			**IR**			**IR + H-NDs**	
			G1	S	G2	G1	S	G2	G1	S	G2
			1.19	0.72	0.48	0.94	0.44	2.22	1.07	0.45	1.55
	ZR75.1$_{Ku70mut}$	Time 12 h	**H-NDs**			**IR**			**IR + H-NDs**	
			G1	S	G2	G1	S	G2	G1	S	G2
			0.12	0.70	0.86	0.89	0.47	2.29	1.03	0.48	1.64
ROS	*Caki-1*	Time 1 h	**H-NDs**			**IR**			**IR + H-NDs**	
			Median			Median			Median	
			2.19			0.89			2.88	
H2AX	*Caki-1*	Time 2 h	**H-NDs**			**IR**			**IR + H-NDs**	
			Median			Median			Median	
			1			12			32	

Fig. 4A, one hour after cell exposure to irradiation alone, the ROS level was not significantly different from the controls (i.e. untreated cells). In contrast, as expected from the H-ND properties, the intracellular level of ROS significantly increased by 2- and 3-fold, after exposure to H-NDs and irradiation, respectively. Interestingly, it appeared that the higher concentration of H-NDs could also induce ROS upon entry into the cells.

2.6. DNA double strand breaks induction (γ-H2AX foci)

To verify whether exposure to H-NDs alone or in combination with irradiation could induce a higher level of DNA DSBs than radiation exposure only, phospho-S129-H2AX (γ-H2AX), a variant of histone H2A, undergoing phosphorylation at DNA DSBs sites, was assayed since it is considered to be the most sensitive marker of DNA DSBs [34–36]. As shown in Fig. 5, the number of γ-H2AX foci after irradiation was higher than the control cells and was found to be stable from 2 to 24 h. Remarkably, exposure to H-NDs alone did not induce γ-H2AX foci in the first couple of hours following exposure but did so later (24 h) at the highest H-ND concentration (64 μg/cm^2).

Combined cell exposure to irradiation (4 Gy) and to H-NDs at low (6 μg/cm^2) and high (64 μg/cm^2) concentrations significantly increased the number of γ-H2AX foci following 2 h of exposure compared to untreated control cells or to cells exposed to radiation alone. However, at 24 h following treatment, the number of γ-H2AX foci, although higher than in control cells, was not significantly different between treatments (i.e. irradiation or H-NDs alone or in combination).

2.7. Late intracellular ROS level

To fully interpret DNA double strand breaks and specifically to understand why H-NDs alone induced DNA breaks at 24 h, we decided to analyze ROS levels 24 h after exposure to H-NDs alone or to H-NDs and radiation combined exposure (Fig. 4B). Moreover the level of DNA damages at 24 h is higher after exposure with H-NDs alone as compared to the combined exposure (Fig. 4A). To verify the

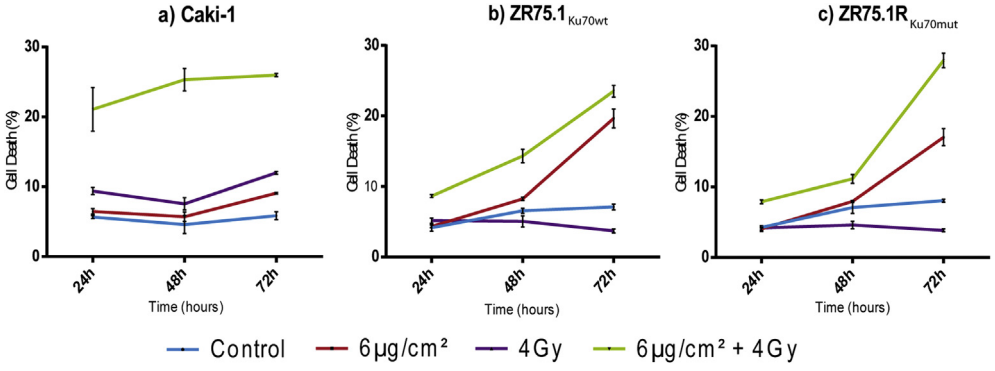

Fig. 2. Cell death induction after H-NDs and/or irradiation treatments. Cell death measurements of a) Caki-1, b) ZR75.1$_{Ku70wt}$ and c) ZR75.1$_{Ku70mut}$ cells, exposed to 6 μg/cm^2 of H-NDs combined or not with irradiation (4 Gy). Cell death induction is represented as the percentage of dead cells among the entire population. Cell counts were taken at 24, 48 and 72 h after treatment. At least 600 cells were counted for each condition. "Control" and "4 Gy" cells were not exposed to H-NDs.

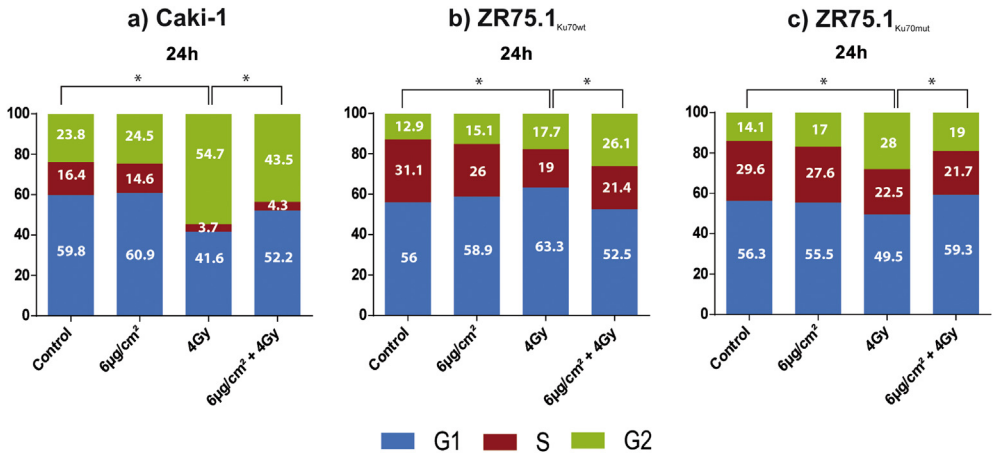

Fig. 3. Cell cycle checkpoint activation following H-NDs and/or irradiation treatments. Cell cycle analysis of a) Caki-1, b) ZR75.1$_{Ku70w}$, and c) ZR75.1 $_{Ku70mut}$ cells exposed to 6 µg/cm^2 of H-NDs combined or not with irradiation (4 Gy). "Control" and "4 Gy" cells were not exposed to H-NDs. Cell cycle checkpoint activation was evaluated by flow cytometry (FacsCalibur) 24 h after treatment. Statistical analysis was performed for each exposure condition compared to non-exposed cells (Student's t-test, *$p < 0.01$).

importance of H-NDs surface for explaining this intriguing result, as a control we compared ROS level after cell exposure to H-NDs or to H-NDs previously irradiated (before any contact with the cells) (Fig. 4B). Overall, it can be seen that i) the ROS level is persistent 24 h after the double exposure to H-NDs and radiation, ii) H-NDs alone induced a slight ROS increase at 24 h and it is effectively related to H-NDs surface since if nanoparticles are irradiated before cell contact, no more ROS are detectable.

The ROS levels observed 24 h after exposure could fully explained DNA double strand breaks at 24 h (Fig. 5).

2.8. Induction of senescence

After 72 h of exposure to H-NDs and irradiation, the cell lines we tested remained in culture without any apparent growth or cell death. Hence, we hypothesized that the senescence can be initiated by persistent DNA damage and act as a barrier to cell proliferation.

Several hallmarks of cellular senescence have been described previously [37–41] including β-galactosidase activation. As shown in Fig. 6A, β-galactosidase activity was found to increase in our three tested cell lines following 7 days of exposure to both H-NDs and radiation. As positive control of senescence, the three cell lines were treated with doxorubicin (140 nM) (Fig. 6C). To further confirm these data, two other markers of senescence were evaluated: the appearance of large persistent γ-H2AX foci and the hypermethylation of a histone H3 (3-methyl-histone-H3K9) that is related to senescence-associated heterochromatinization (SAH). Representative images of the labeling of these two markers are presented in Fig. 6B. These results clearly demonstrated that at 7 days after co-exposure to H-NDs (6 µg/cm^2) and gamma rays (4 Gy), Caki-1 cells displayed large γ-H2AX foci (green labeling) and the increased labeling of 3-methyl-Histone H3K9 (red labeling), indicating irreversibly entry into senescence.

To further highlight the potentialization of co-treatment with H-NDs and irradiation, the ratios of the obtained results between the samples and controls were compiled for all performed tests. These

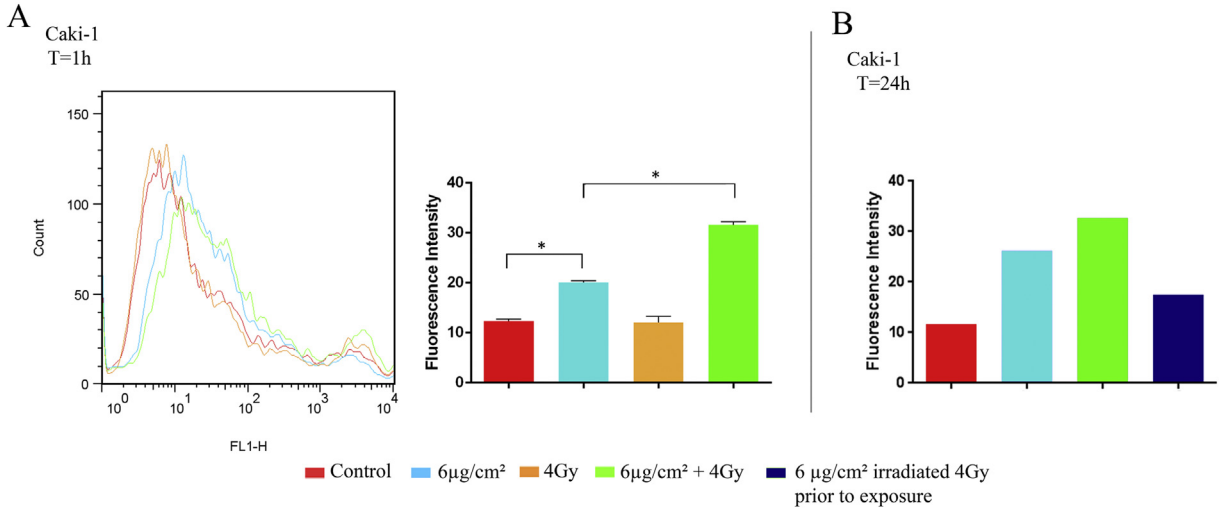

Fig. 4. Intracellular generation of reactive oxygen species (ROS) by H-NDs and/or irradiation treatments. (A) Caki-1 cells were treated for 1 h with H-NDs (6 µg/cm^2) alone (blue) or in combination with irradiation (green). Control (basal level, red) and 4 Gy (orange) cells were not exposed to H-NDs. The ROS level was monitored by measurement of the fluorescence intensity (arbitrary units) of an oxidized fluorescent probe. The left part of the figure presents curves obtained after flow cytometry analysis. For the right part, the median fluorescence intensity of each sample is recorded. Statistical analysis was performed for each exposure condition compared to non-exposed cells (Student's t-test, *$p < 0.01$). (B) Caki-1 cells were treated were treated for 24 h in the same conditions and with H-NDs (6 µg/cm^2) irradiated at 4 Gy prior to exposure.

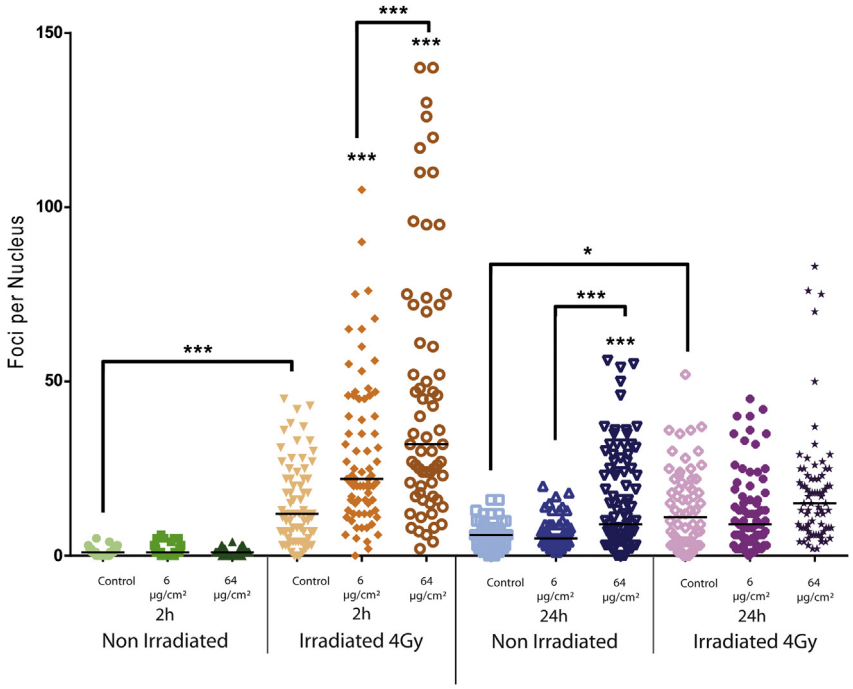

Fig. 5. H-ND genotoxicity measured by γ-H2Ax foci counts. γ-H2Ax foci were counted in Caki-1 cells exposed to H-NDs in combination or not with irradiation (4 Gy), for 2 and 24 h "Control" cells were not exposed to H-NDs. Counts were performed on at least 100 cells per condition and results are depicted as dot plot distribution values of the number of foci obtained for each tested condition (the median is also reported for each sample). A Wilcoxon rank test (comparisons versus control cells not exposed to NPs) was used to determine statistical significance (*, $p < 0.05$; **, $p < 0.01$; ***, $p < 0.001$).

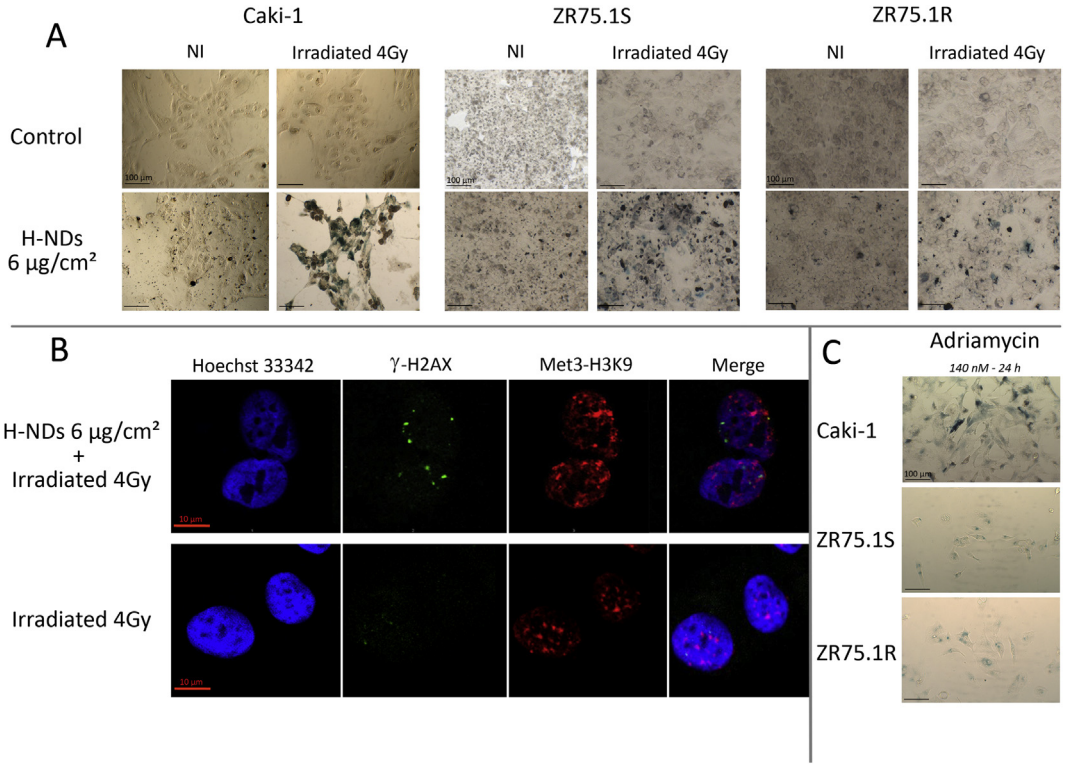

Fig. 6. (A) Induction of β-galactosidase activity following cotreatment with H-NDs and irradiation. β-galactosidase activity measurements in a) Caki-1, b) ZR75.1S, and c) ZR75.1R cell lines exposed for 7 days to H-NDs in combination or not with irradiation (4 Gy). Control cells were not exposed to H-NDs. (B) Measurement of senescence associated heterochromatinization (SAH) and the induction of persistent large γ-H2Ax foci in cells treated with H-NDs and irradiation. Caki-1 cells were exposed for 7 days to a) H-NDs (6 µg/cm^2) combined with irradiation (4 Gy) or b) irradiation (4 Gy) only. (C) Positive control of senescence induction. All three cell lines have been exposed to adryamycin (140 nM) for 24 h.

ratios, indicated in Table 2, were calculated for the time points at which the observed effects were the most obvious. This allowed us to convert all of our previously described results into real number values. Indeed, these ratios were found to be consistent with our first hypothesis i.e. the co-exposure of cells to H-NDs and irradiation is a valid strategy for overcoming the radio-resistance of cancer cells.

As an illustration of our aforementioned observations, we calculated the cellular index ratios for each condition following 160 h of exposure (Table 2). Samples treated with H-NDs or radiation alone were compared to the control and those exposed to H-NDs and radiation were compared to the irradiated sample. These initial biological data suggested that the deleterious effects of DNA DSBs produced either by NCS or ionizing irradiation can be amplified by H-NDs.

3. Discussion

Our current data provide robust evidence for the potentialization of ionizing irradiation by H-NDs at doses as low as 6 $\mu g/cm^2$; in parallel, H-NDs alone do not induce any cell cytotoxicity after 48 h of exposure at doses up to 96 $\mu g/cm^2$. These data are also consistent with the absence of ND toxicity already described in some studies of detonation ND biokinetics for 100 fold higher concentrations [42].

The co-exposure (H-NDs and radiation) leads to a higher level of intracellular ROS than either single treatment. Based on their characteristics, H-NDs in an aqueous environment are expected to adsorb a high level of oxygen-related species [43], thus acting as a potential source of ROS if activated by electron photoemission via ionizing radiation. Ionizing radiation is known to induce very early and transiently intra-cellular ROS that are no longer detectable at 30 min after exposure [44], explaining why we could not quantify any intra-cellular ROS 1 h after exposure. It also confirms the high level of oxidative stress generated within the cells by H-NDs especially after double treatment. Furthermore, the ROS level measured 1 h after treatment highlights a sustained production of ROS. Thus, the higher cytotoxic effect observed after the double exposure, in terms of cell death and cell cycle could be related to the increased ROS level generated by both H-NDs and irradiation.

This hypothesis is also compatible with data obtained when cells are exposed to both H-NDs and the radiomimetic drug neocarzinostatin (Supplementary Data 1). This drug physically interacts with DNA through its chromophore moiety and this interaction is followed by thiol activation and the ROS-dependent generation of carbon-centered radicals on deoxyribose [45–47]. Given that ionizing irradiation or neocarzinostatin induce both DNA SSBs and DSBs, through direct energy deposition and also indirectly through ROS generation followed by DNA alkylation, a second source of sustained ROS production (that may be otherwise tolerated by cells) generated by H-NDs may result in increased and sustained DNA damage.

The activation of a G_1/S cell cycle checkpoint also appears to be a specific effect of this associated cell treatment, as a consequence of a concomitant increase in DNA SSBs occurring in G_1 phase following the generation of ROS. DNA DSBs and SSBs are induced directly by ionizing radiation through energy deposition [33]. Indirectly, ionizing radiation also induces ROS (i.e. through water radiolysis) that alkylates DNA bases resulting in SSBs. These SSBs, if unrepaired, could lead to DSBs. This finding was consistent with the number of unrepaired DNA breaks that cause both G_1 and G_2/M cell cycle arrest (Fig. 3).

Our results suggested that ROS are spontaneously generated or induced once H-NDs enter the cells at a level that persists and is high enough to continuously induce DNA DSBs. In fact, considering that cells exposed to H-NDs (at the highest concentration) alone showed a higher rate of γ-H2AX foci than control cells after 24 h, one could postulate a higher level of DNA DSB at this time point in cells co-exposed to H-NDs and to irradiation. Two non-exclusive hypotheses could arise as explanations: i) at 24 h after exposure, about 20% of Caki-1 cells have died, as assessed by trypan blue staining, and it can be assumed that these cells contained higher numbers of DNA breaks; or ii) once the cell is irradiated, H-NDs can no longer generate ROS and therefore do not induce DNA breaks in addition to those induced by irradiation alone. This second hypothesis has been confirmed in our current analyses, since the ROS level quantified in the cells exposed to H-NDs and irradiated prior to exposure was 50% lower than that measured in cells exposed to H-NDs alone (see Supplementary Data 2).

Consequently, we hypothesize that the cooperation between H-NDs and irradiation leads to a global increase in DNA SSBs and DSBs, in both cases initiated by ROS. In addition, DSBs initiated in this way may further contribute to *de novo* ROS generation [48]. These repeated loop-reactions might explain why persistent and large γ-H2AX foci were observed in cells exposed to both H-NDs and irradiation (Fig. 6B). Most importantly, following the same type of double cell treatment, we show from our results that activation of a G_1/S cell cycle checkpoint occurs in parallel with a G_2/M release initiated by irradiation exposure (Fig. 5). These two findings are consistent with the relatively low level of cell death we observed and indicate a predominant senescence process since it has been reported that sustained SSBs may also initiate γ-H2AX foci formation through chromatin structural reorganization [49].

The final outcome of this combination treatment is cellular senescence, a finding that may be of particular relevance for advancing future radiotherapy regimens, most notably the possibility of reducing the dose of irradiation and also overcoming the resistance of certain cancer cells to this therapy.

The activation of senescence by otherwise sub-lethal doses of irradiation is of particular interest and our results highlight a potentiation effect of H-NDs on irradiation in radio-resistant cells which has promising implications for future clinical approaches. Effectively the induction of senescence has been proposed as a potent tumor-suppressive irreversible process of particular interest in cases where chemo- and/or radio-therapy fail to induce cell death [50,51]. In this work we presented initiation of senescence as the final biological effect of H-NDs and irradiation in cancer cell lines displaying functional p53. In few other cell lines expressing mutated p53 or being p53 deficient, we did not observed senescence but rather increased cell death (data not shown).

Finally, all these biological effects resulting from H-NDs exposed to irradiation goes in line with the current and strong scientific emulation around hydrogenated diamond. Indeed, recent works of Hamers et al. summarized the possibility to easily photo-generate solvated electrons and/or radicals from its surface, opening the way to new promising applications for diamond, notably toward photo-catalysis [52,53]. In this context, we demonstrated here for the first time the potential of hydrogenated nanodiamond for radiosensitization of tumor cells. Compared to metallic high-Z nanoparticles (gold NPs, HfO_2 NPs), widely studied today because of their high photon absorption and consecutive radiation–matter interactions, H-NDs present several assets: (i) they benefit from their semiconductor behavior and negative electron affinity to photo-emit directly low-energy electrons into the surrounding medium, (ii) they exhibit a native positive zeta potential without any coating and (iii) they are surrounded with high amount of adsorbed oxygen-containing molecules [20]. H-NDs have promise indeed in improving the treatment of radiation resistant tumors but also could have impact on the radio-sensitive tumors by enabling lower doses of ionizing radiations to be used and thus

potentially reducing adverse side effects. For all these reasons, H-ND definitely constitutes a valuable candidate as radiosensitizing agent possibly associated with antisense molecular therapy.

4. Methods

4.1. Nanodiamonds

Detonation nanodiamonds (NDs) were provided by the Nanocarbon Research Institute.

4.2. Plasma hydrogenation of nanodiamonds

80-100 mg of NDs were deposited in a quartz tube and inserted in a plasma Downstream source (Sairem). High purity research grade N9.0 hydrogen gas was injected in the tube at a pressure of 15 mbar and plasma was generated in the quartz tube with a microwave power of 300 W (2.45 GHz). During the plasma, the tube was air cooled and a smooth rotation is applied in order to mix the particles in the plasma. NDs were exposed to hydrogen plasma for 15 min and were cooled down under hydrogen, leading to H-NDs.

4.3. Preparation of nanodiamonds dispersions

H-NDs were dispersed in ultrapure water by sonication (Hielscher UP400S, 300W, 24 kHz) for 2h under cooling. Larger aggregates were removed from the solution by 1 h centrifugation at 4000 rpm. NDs are resuspended in water and not in PBS solution, that could be more compatible with cells, because too get its positive zeta potential and to disaggregate them, H-NDs need to be first sonicated in pure water. This is not possible directly in PBS due to its very high ionic strength.

4.4. Cell lines and cell culture

Caki-1 (ATCC number: HTB-46^{TM}) and ZR75.1 cells were routinely grown at 37 °C in a humidified atmosphere of 5% CO_2 and 95% air, in Dulbecco's modified Eagle medium (DMEM) glutumax supplemented with 10% (v/v) heat-inactivated fetal bovine serum (Sigma–Aldrich),1 mM penicillin-streptomycin (Invitrogen) and 1% (v/v) non-essential amino acids (Invitrogen). ZR75.1 cells (ATCC number: CRL-1500^{TM}) were transfected using Amaxa Nucleofector (Lonza, France) with vectors containing cDNAs for the non-homologous end-joining DNA repair protein Ku70 as described elsewhere (Bouley et al., submitted). Stable populations of cells expressing either wild type or mutant Ku70 were established under hygromycin selection (125 μg/mL).

4.5. γ-Ionizing irradiation

Cells were irradiated immediately after being exposed to H-NDs in a ^{137}Cs source irradiation unit (IBL637, CisBio International, Gif sur Yvette, France) at 1.61 Gy min^{-1}. We used 4 Gy which has previously been reported as a sub-toxic dose [54,55], (Bouley et al., submitted).

4.6. xCELLigence® real-time follow-up

Refer to Supplementary Data.

4.7. Determination of cell toxicity (trypan blue)

After treatments, dead cells were counted after 24, 48 and 72 h of exposure. At each time point, adherent cells and supernatant were collected. For each sample, at least 600 cells were counted (living and dead cells) in a 50% V/V dilution of 0.04% Trypan Blue Solution (Sigma), to obtain the percentage of dead cells in the complete population.

4.8. Cell cycle check-points

Following 6, 12, 24 and 48 h of exposure, the supernatant was removed, and the cells were washed and trypsinized for 5 min. Cells were suspended at a density of 10^6 cells/ml in PBS, fixed in 3 volumes of 70% ethanol (50% final concentration) and then incubated for 30 min at 4 °C. After centrifugation at for 5 min at 300 × g at 4 °C and 3 times washes in PBS, cells were treated with RNase A (DNase free) at a final concentration of 0.3 mg/ml in PBS and propidium iodide (PI) to a final concentration of 20 μg/ml. PI fluorescence was analyzed on a standard FacsCalibur (BD Biosciences, San Jose, CA) with log acquisition in the FL2 (585/42 nm) channel after doublet discrimination. Statistical analysis of data was performed using FlowJo software (Treestar, Ashland, OR).

4.9. Measurement of reactive oxygen species (ROS)

15×10^4 Caki-1 cells were seeded on 6 well plates (TPP) at least 27 h before exposure. After treatment, supplier's instructions were followed to measure ROS intra-cellular level with CM-H2DCFDA probe (Life Technologies). ROS level was analyzed on a standard FacsCalibur (BD Biosciences, San Jose, CA) with log acquisition in the FL1 (530/30 nm) channel. Statistical analysis of the data was performed using FlowJo software (Treestar, Ashland, OR).

4.10. Genotoxicity and confocal microscopy γ −H2AX foci count

Refer to Supplementary Data.

4.11. Induction of senescence: measurement of β-galactosidase activity and senescence associated heterochromatinization (SAH)

Refer to Supplementary Data.

Author contributions

The author contributions were as follows – SC, JCA, JD and RG designed the research. HAG, TP, JCA, CG and MCS conducted the synthesis and characterization of H-NDs. RG, JD, VP and LS conducted the biological and biochemical experiments. SC, JCA, HAG, JD and RG wrote the manuscript. All authors critically read and approved the final version of the manuscript.

Conflict of interest

The authors declare no competing conflict of interests.

Acknowledgments

This work was funded by the French national research program NANOTRANS, the NanoSciences and Technology pour la Santé CEA-Transverse programs, the Dim C'Nano IdF (CP09-462), the EU Framework 7 Programme NANoREG 1 (310.584) and the French Agency for Food, Environmental and Occupational Health Safety (ANSES) (EST-2011/1/036). RG is a recipient of a fellowship from ANSES.

Appendix A. Supplementary data

Supplementary data related to this article can be found at http://dx.doi.org/10.1016/j.biomaterials.2015.05.034.

References

[1] K.K. Liu, W.W. Zheng, C.C. Wang, Y.C. Chiu, C.L. Cheng, Y.S. Lo, et al., Covalent linkage of nanodiamond-paclitaxel for drug delivery and cancer therapy, Nanotechnology 21 (2010) 315106.

[2] J. Li, Y. Zhu, W. Li, X. Zhang, Y. Peng, Q. Huang, Nanodiamonds as intracellular transporters of chemotherapeutic drug, Biomaterials 31 (2010) 8410–8418.

[3] E.K. Chow, X.Q. Zhang, M. Chen, R. Lam, E. Robinson, H. Huang, et al., Nanodiamond therapeutic delivery agents mediate enhanced chemoresistant tumor treatment, Sci. Transl. Med. 3 (2011) 73ra21.

[4] J.I. Chao, E. Perevedentseva, P.H. Chung, K.K. Liu, C.Y. Cheng, C.C. Chang, et al., Nanometer-sized diamond particle as a probe for biolabeling, Biophys. J. 93 (2007) 2199–2208.

[5] V. Paget, J.A. Sergent, R. Grall, S. Altmeyer-Morel, H.A. Girard, T. Petit, et al., Carboxylated nanodiamonds are neither cytotoxic nor genotoxic on liver, kidney, intestine and lung human cell lines, Nanotoxicology 8 (S1) (August 2014) 46–56.

[6] S.J. Yu, M.W. Kang, H.C. Chang, K.M. Chen, Y.C. Yu, Bright fluorescent nanodiamonds: no photobleaching and low cytotoxicity, J. Am. Chem. Soc. 127 (2005) 17604–17605.

[7] Y.R. Chang, H.Y. Lee, K. Chen, C.C. Chang, D.S. Tsai, C.C. Fu, et al., Mass production and dynamic imaging of fluorescent nanodiamonds, Nat. Nanotechnol. 3 (2008) 284–288.

[8] U. Maitra, A. Jain, S.J. George, C.N. Rao, Tunable fluorescence in chromophore-functionalized nanodiamond induced by energy transfer, Nanoscale 3 (2011) 3192–3197.

[9] A.M. Schrand, J.B. Lin, S.C. Hens, S.M. Hussain, Temporal and mechanistic tracking of cellular uptake dynamics with novel surface fluorophore-bound nanodiamonds, Nanoscale 3 (2011) 435–445.

[10] I.P. Chang, K.C. Hwang, C.S. Chiang, Preparation of fluorescent magnetic nanodiamonds and cellular imaging, J. Am. Chem. Soc. 130 (2008) 15476–15481.

[11] A. Alhaddad, M.P. Adam, J. Botsoa, G. Dantelle, S. Perruchas, T. Gacoin, et al., Nanodiamond as a vector for siRNA delivery to Ewing sarcoma cells, Small 7 (2011) 3087–3095.

[12] H.A. Girard, T. Petit, S. Perruchas, T. Gacoin, C. Gesset, J.C. Arnault, et al., Surface properties of hydrogenated nanodiamonds: a chemical investigation, Phys. Chem. Chem. Phys. 13 (2011) 11517–11523.

[13] H. Huang, E. Pierstorff, E. Osawa, D. Ho, Active nanodiamond hydrogels for chemotherapeutic delivery, Nano Lett. 7 (2007) 3305–3314.

[14] A. Krueger, D. Lang, Functionality is Key: recent Progress in the Surface Modification of Nanodiamond, Adv. Funct. Mater. 22 (2012) 890–906.

[15] V.N. Mochalin, O. Shenderova, D. Ho, Y. Gogotsi, The properties and applications of nanodiamonds, Nat. Nanotechnol. 7 (2012) 11–23.

[16] T. Petit, J.C. Arnault, H.A. Girard, M. Sennour, T.Y. Kang, C.L. Cheng, et al., Oxygen hole doping of nanodiamond, Nanoscale 4 (2012) 6792–6799.

[17] V.Y. Dolmatov, Detonation-synthesis nanodiamonds: synthesis, structure, properties and applications, Russ. Chem. Rev. 76 (2007) 339–360.

[18] J.C. Arnault, T. Petit, H. Girard, A. Chavanne, C. Gesset, M. Sennour, et al., Surface chemical modifications and surface reactivity of nanodiamonds hydrogenated by CVD plasma, Phys. Chem. Chem. Phys. 13 (2011) 11481–11487.

[19] H.A. Girard, J.C. Arnault, S. Perruchas, S. Saada, T. Gacoin, J.P. Boilot, et al., Hydrogenation of nanodiamonds using MPCVD: A new route toward organic functionalization, Diam. Relat. Mater. 19 (2010) 1117–1123.

[20] T. Petit, H.A. Girard, A. Trouve, I. Batonneau-Gener, P. Bergonzo, J.C. Arnault, Surface transfer doping can mediate both colloidal stability and self-assembly of nanodiamonds, Nanoscale 5 (2013) 8958–8962.

[21] A. Alhaddad, C. Durieu, G. Dantelle, E. Le Cam, C. Malvy, F. Treussart, et al., Influence of the internalization pathway on the efficacy of siRNA delivery by cationic fluorescent nanodiamonds in the Ewing sarcoma cell model, PloS one 7 (2012) e52207.

[22] M.Z. Chen, Q. X, H.B. Man, R. Lam, E.K. Chow, D. Ho, Nanodiamond Vectors Functionalized with Polyethylenimine for siRNA Delivery, J. Phys. Chem. Lett. 1 (2010) 3087–3095.

[23] A. Gismondi, G. Reina, S. Orlanducci, F. Mizzoni, S. Gay, M.L. Terranova, et al., Nanodiamonds coupled with plant bioactive metabolites: a nanotech approach for cancer therapy, Biomaterials 38 (2015) 22–35.

[24] J.B. Cui, J. R, L. Ley, Electron affinity of the bare and hydrogen covered single crystal diamond, Surf. Phys. Rev. Lett. 81 (1998) 429–432.

[25] I. Kondo TN, V.N. Mochalin, J. Urai, M. Yuasa, Y. Gogotsi, Electrical conductivity of thermally hydrogenated nanodiamond powders, J. Appl. Phys. 113 (2013).

[26] K. Rezwan, A.R. Studart, J. Voros, L.J. Gauckler, Change of zeta potential of biocompatible colloidal oxide particles upon adsorption of bovine serum albumin and lysozyme, J. Phys. Chem. B 109 (2005) 14469–14474.

[27] H. Yogasundaram, M.S. Bahniuk, H.D. Singh, H.M. Aliabadi, H. Uludag, L.D. Unsworth, BSA Nanoparticles for siRNA Delivery: Coating Effects on Nanoparticle Properties, Plasma Protein Adsorption, and In Vitro siRNA Delivery, Int. J. Biomaterials 2012 (2012) 584060.

[28] O. Dreesen, A. Chojnowski, P.F. Ong, T.Y. Zhao, J.E. Common, D. Lunny, et al., Lamin B1 fluctuations have differential effects on cellular proliferation and senescence, J. Cell Biol. 200 (2013) 605–617.

[29] W. Stallaert, J.F. Dorn, E. van der Westhuizen, M. Audet, M. Bouvier, Impedance responses reveal beta(2)-adrenergic receptor signaling pluridimensionality and allow classification of ligands with distinct signaling profiles, PloS One 7 (2012) e29420.

[30] N. Ke, X. Wang, X. Xu, Y.A. Abassi, The xCELLigence system for real-time and label-free monitoring of cell viability, Methods Mol. Biol. 740 (2011) 33–43.

[31] H.Y. Nam, M.W. Han, H.W. Chang, Y.S. Lee, M. Lee, H.J. Lee, et al., Radioresistant cancer cells can be conditioned to enter senescence by mTOR inhibition, Cancer Res. 73 (2013) 4267–4277.

[32] D. Deckbar, P.A. Jeggo, M. Lobrich, Understanding the limitations of radiation-induced cell cycle checkpoints, Crit. Rev. Biochem. Mol. Biol. 46 (2011) 271–283.

[33] P. Jeggo, M. Lobrich, Radiation-induced DNA damage responses, Radiat. Prot. Dosim. 122 (2006) 124–127.

[34] C.E. Redon, A.J. Nakamura, O.A. Martin, P.R. Parekh, U.S. Weyemi, W.M. Bonner, Recent developments in the use of gamma-H2AX as a quantitative DNA double-strand break biomarker, Aging (Albany NY) 3 (2011) 168–174.

[35] R. Scully, A. Xie, Double strand break repair functions of histone H2AX, Mutat. Res. 750 (2013) 5–14.

[36] D.J. Smart, K.P. Ahmedi, J.S. Harvey, A.M. Lynch, Genotoxicity screening via the gammaH2AX by flow assay, Mutat. Res. 715 (2011) 25–31.

[37] J. Campisi, Cellular senescence: putting the paradoxes in perspective, Curr. Opin. Genet. Dev. 21 (2011) 107–112.

[38] J.R. Dorr, Y. Yu, M. Milanovic, G. Beuster, C. Zasada, J.H. Dabritz, et al., Synthetic lethal metabolic targeting of cellular senescence in cancer therapy, Nature 501 (2013) 421–425.

[39] K.M. Aird, R. Zhang, Detection of senescence-associated heterochromatin foci (SAHF), Methods Mol. Biol. 965 (2013) 185–196.

[40] Z. Tu, K.M. Aird, R. Zhang, Chromatin remodeling, BRCA1, SAHF and cellular senescence, Cell. Cycle 12 (2013) 1653–1654.

[41] M. Yamauchi, Y. Oka, M. Yamamoto, K. Niimura, M. Uchida, S. Kodama, et al., Growth of persistent foci of DNA damage checkpoint factors is essential for amplification of G1 checkpoint signaling, DNA Repair 7 (2008) 405–417.

[42] R. Kaur, I. Badea, Nanodiamonds as novel nanomaterials for biomedical applications: drug delivery and imaging systems, Int. J. Nanomedicine 8 (2013) 203–220.

[43] V. Chakrapani, J.C. Angus, A.B. Anderson, S.D. Wolter, B.R. Stoner, G.U. Sumanasekera, Charge transfer equilibria between diamond and an aqueous oxygen electrochemical redox couple, Science 318 (2007) 1424–1430.

[44] M. Diehn, R.W. Cho, N.A. Lobo, T. Kalisky, M.J. Dorie, A.N. Kulp, et al., Association of reactive oxygen species levels and radioresistance in cancer stem cells, Nature 458 (2009) 780–783.

[45] I.H. Goldberg, Free radical mechanisms in neocarzinostatin-induced DNA damage, Free Radic. Biol. Med. 3 (1987) 41–54.

[46] L.S. Kappen, T.R. Lee, C.C. Yang, I.H. Goldberg, Oxygen transfer from the nitro group of a nitroaromatic radiosensitizer to a DNA sugar damage product, Biochemistry 28 (1989) 4540–4542.

[47] Y. Kwon, Z. Xi, L.S. Kappen, I.H. Goldberg, X. Gao, New complex of post-activated neocarzinostatin chromophore with DNA: bulge DNA binding from the minor groove, Biochemistry 42 (2003) 1186–1198.

[48] M.A. Kang, E.Y. So, A.L. Simons, D.R. Spitz, T. Ouchi, DNA damage induces reactive oxygen species generation through the H2AX-Nox1/Rac1 pathway, Cell Death Dis. 3 (2012) e249.

[49] J.P. Banath, C.A. Banuelos, D. Klokov, S.M. MacPhail, P.M. Lansdorp, P.L. Olive, Explanation for excessive DNA single-strand breaks and endogenous repair foci in pluripotent mouse embryonic stem cells, Exp. Cell Res. 315 (2009) 1505–1520.

[50] J. Campisi, Cellular senescence as a tumor-suppressor mechanism, Trends Cell. Biol. 11 (2001) S27–S31.

[51] J. Campisi, J.K. Andersen, P. Kapahi, S. Melov, Cellular senescence: a link between cancer and age-related degenerative disease? Semin. Cancer Biol. 21 (2011) 354–359.

[52] D. Zhu, L. Zhang, R.E. Ruther, R.J. Hamers, Photo-illuminated diamond as a solid-state source of solvated electrons in water for nitrogen reduction, Nat. Mater. 12 (2013) 836–841.

[53] L. Zhang, D. Zhu, G.M. Nathanson, R.J. Hamers, Selective photoelectrochemical reduction of aqueous CO(2) to CO by solvated electrons, Angew. Chem. Int. Ed. Engl. 53 (2014) 9746–9750.

[54] S. Ning, K. Trisler, B.W. Wessels, S.J. Knox, Radiobiologic studies of radioimmunotherapy and external beam radiotherapy in vitro and in vivo in human renal cell carcinoma xenografts, Cancer 80 (1997) 2519–2528.

[55] A. Smyth, H.M. Reid, A.H. Baker, H. McGlynn, Modifications of the radiosensitivity of a renal cancer cell line as a consequence of stable TIMP-1 overexpression, Int. J. Radiat. Biol. 83 (2007) 13–25.